



Process parameters optimization of differential heating push-bending for small bending radius tube based on orthogonal experiments

Mingliang Peng¹ · Xuefeng Xu¹ · Yubin Fan¹ · Jie Xiao¹ · Liming Wei² · Jun Xie² · Dong Yang¹

Received: 9 November 2023 / Accepted: 26 May 2024 / Published online: 13 June 2024
© The Author(s), under exclusive licence to Springer-Verlag London Ltd., part of Springer Nature 2024

Abstract

A process of differential heating push-bending (DHP-B) was proposed to enhance the forming quality of thin-walled tubes with small bending radius. Finite element numerical simulation and the orthogonal test method were employed to optimize the process parameters, including temperature, friction coefficients of the inner and outer deformation zones (Z_1 and Z_2) as well as the guide zone (Z_3), and the reverse thrust, for bending 5A02 aluminum alloy tubes with a diameter of 32 mm, a wall thickness of 1 mm, and a relative bending radius of 0.9. The thinning rate, ovality, and push-out amount were taken as the evaluation indexes to determine the primary and secondary relationships between the factors by the comprehensive balance method. Temperature, among these factors, had the most significant impact on these evaluation indexes. The variation of friction coefficient mainly affected thinning rate and ovality, whereas the reverse thrust primarily affected the push-out amount. The optimal parameter combinations were identified as a temperature of 300 °C, friction coefficient Z_1 of 0.1, Z_2 of 0.1, Z_3 of 0.03, and reverse thrust of 27 MPa, as revealed by the results. Finally, the simulation results were validated by experiments.

Keywords Thin-walled tubes with small bending radius · Differential heating push-bending · Forming quality · Finite element simulation · Orthogonal experiment

1 Introduction

Thin-walled tubes with small bending radius, which are defined as the ratio of wall thickness to outer diameter (t/D) is smaller than 0.05 and the ratio of bending radius to outer diameter (R/D) is smaller than 1.5, are widely used in aerospace, marine, automotive, petroleum, and other engineering fields due to their optimized layout, compact structure, and lightweight characteristics [1–4]. Push-bending is a significant method to form thin-walled tubes with a small bending radius. During the process of push-bending, as the relative bending radius decreases, thin-walled tubes cause the defects such as wrinkling, over-thinning, and cross-section distortion that is more prone to occur in the bending process [5, 6]. As such, studying the forming defects in the bending

process of thin-walled tubes, analyzing the mechanism of tube bending deformation and wrinkling, and comprehending the impact of forming parameters on the forming quality law are imperative [7].

In the field of hot-forming processes, temperature is a crucial influential parameter. Zhang et al. [8] optimized heat-assisted rotary draw bending parameters for high-strength titanium alloy tubes with small bending radius. Their investigation found that temperature affects bent tube cross-section distortion and over-wall thinning. Xu et al. [9] investigated the effect of different temperatures (400 °C, 425 °C, 450 °C, and 475 °C) on the forming properties of 6063 aluminum alloy tubes, discovered that the expansion rate of the part increases with the forming temperature, and that the metal hot forming process significantly improves the forming properties of tubes. Zhang et al. [10, 11] suggested a thermo-mechanical three-dimensional finite element (3D-FE) model for LDTW CP-Ti tube preheating and heat bending. Simulations examined how preheating temperature affected bending die temperature distribution and tube wall thickness. Wu et al. [12, 13] examined the impact of temperature on the bendability of AM30 tubes, revealing that moderate temperatures positively influenced the thermal bending quality.

✉ Xuefeng Xu
xfwinzy@163.com

¹ School of Aviation Manufacturing Engineering, Nanchang Hangkong University, Nanchang, Jiangxi 330063, PR China

² School of National Demonstration Center for Experimental Engineering Training Education, Nanchang Hangkong University, Nanchang, Jiangxi 330063, PR China

Tao et al. [14] used a thermal-mechanical coupling finite element model to study Ti-6Al-4 V tube warm-bending. After examining tube quality and bending efficiency, the researchers discovered the best heating technique. Li et al. [15] constructed a complete elastic-plastic and thermo-mechanical model to study pipe bending under local heating or cooling. FEM simulations examined metal deformation during bending, including pipe wall thickness thinning and thickening. Chavoshi et al. [16] investigated Spot Heating's deformation for pipe straightening. Optimizing heating parameters within a thick pipe wall helps develop the shortening mechanism. Pipe curvature increased significantly. Tran et al. [17] investigated the superplastic thermoforming process of hot tubes, conducting tests at a forming temperature of 900 °C, and successfully fabricated a Ti-3Al-2.5 V titanium alloy helically shaped flex tube with a uniform wall thickness distribution. Hence, it can be inferred that heating facilitates the reduction of process defects and enhances the forming quality of formed parts. By the way, it can also be concluded that the lower the friction coefficient was, the bigger the thickness of the thickening area.

In contrast to the existing monolithic heating form, numerous scholars have further focused on the improvement of the process by selectively heating specific areas to create differential heating in response to the non-uniformity of the forming. Hoffmann et al. [18] investigated how partial cross-sectional heating affected L-profile warping and spring back during three-roll push-bending. Experimental methods reveal that the temperature differential between heated and room temperatures displaces stress-free fibers, reducing warping. Yan et al. [19, 20] proposed a technique for forming tubes through differential temperature shear and bending. Ti-alloy thin-walled tubes were heated during forming to increase the shear and bending deformation capabilities of the tube. Simultaneously, the straight section of the tube was cooled with airflow to decrease the temperature of the load-bearing zone, thereby increasing the load-bearing capacity of the zone and ultimately improving the tube's bending forming limit. Hu [21] created a finite element (FE) model to simulate the process of local induction-heating bending of pipes with a small bending radius, specifically with a ratio of bending radius to pipe diameter (R/D) equal to 1.5. Local induction heating is used to analyze mechanical loads and strains during large-pipe bending. Vorkov et al. [22] used radiant heating from infrared lamps to locally heat the plates. Radiant heating also reduced the bending force and, consequently, the spring back and bend allowance. Schlemmer et al. [23] revealed the selective enhancement of metal flow in certain places that have been locally heated. This mechanism confers significant benefits in terms of component strength and fatigue parameters. Liu et al. [24] presented warm hydroforming using a non-uniform temperature field. This technology addressed

heated hydroforming's thickness uniformity and expansion ratio concerns. An adequate temperature difference reduces feeding zone thickening and improves tubular component thickness uniformity. Guo et al. [25] used the finite element technique to model and analyze the bending process of P11 alloy steel pipes using local-induction heating. The findings from the simulation demonstrated that the manipulation of heating settings had a significant impact on the outcome of the forming process. Simonetto et al. [26] used numerical simulation to study how selective heating affects thin-walled titanium alloy tube rotary drawing. The results show that selective heating can improve bent tube quality. Yang et al. [27] examined titanium tube differential heating-based rotational draw bending. Overall heating increased titanium tube work hardening. They observed that the application of work hardening reduced bending wrinkling. Therefore, the DHP-B forming method proposed in this paper coincides with the differential heating shear bending, the differential heating deep drawing, and other heating processes. The DHP-B forming process may improve forming quality.

Aiming to improve wall thickening at the intrados and wall thinning at the extrados, the DHP-B method of thin-walled tubes with small bending radius was studied in this paper, and the influence of forming parameters on forming quality was analyzed. Eventually, the process parameters were optimized by the orthogonal test method.

2 Principle and indices of DHP-B

Metal materials soften when heated [28], which leads to a in yield strength but an increase in formability. By introducing a temperature field to heat the extrados of the tube, it was able to make the material more fluid and reduce the risk of thinning and rupture on the extrados. Meanwhile, the intrados was kept at room temperature to maintain rigidity, improving material strength and reducing the risk of thickening and wrinkling on the intrados. To control the temperature, heating rods were added to the outer side of the die and cooling tank was set on the inside of the die. Water passed through the tank, then the inner side of the die was cooled, and different temperatures of the die were generated, as shown in Fig. 1. The punch provides the thrust to bend the tube blank along the contours of the cavity, propelling the flexible rod in the opposite direction through the subdivided elastic rubber. The combined force of F_1 and F_2 pressurizes the rubber to bolster the tube.

The ovality of the cross-section and wall thickness variation are the crucial factors affecting the forming quality of thin-walled tubes with small bending radius. The ovality and wall thickness distribution are shown in Fig. 2. The maximum ovality γ , maximum thickening rate δ , and maximum thinning rate ε can be calculated by Eq. (1) to Eq. (3).

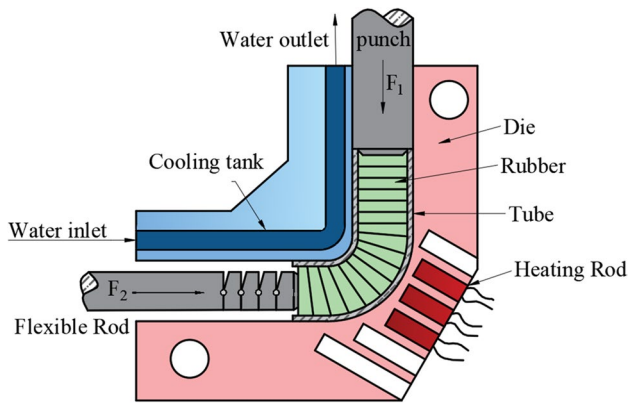


Fig. 1 Schematic diagram of DHP-B forming

$$\gamma = \frac{d_{max} - d_{min}}{d_0} \times 100\% \tag{1}$$

$$\delta = \frac{t_{max} - t_0}{t_0} \times 100\% \tag{2}$$

$$\epsilon = \frac{t_0 - t_{min}}{t_0} \times 100\% \tag{3}$$

where t_0 and d_0 represent the initial wall thickness and outer diameter of the tube, while t_{max} , t_{min} , and d_{min} denote respectively the maximum inner wall thickness, minimum outer wall thickness, and minimum axis of the bent tube.

In the DHP-B simulation, the temperature of the tube decreases gradually from the extrados to the intrados of the bend, resulting in a reasonable distribution of the rigid-plastic

deformation in each deformation region during the bending of the tube blank. In order to achieve the goal of appropriate temperature distribution of the tube blank, a theoretical analysis was conducted on the heat conduction between the heating rod and the die, as well as the heat transfer between the die and the tube.

Implementing an indirect heating approach for the tube blank involves calculating the thermal conduction between the heating rod and the die. In Abaqus, the equation utilized for simulating thermal conduction issues is known as the heat conduction equation, also referred to as the heat diffusion equation shown in Eq. (4).

$$\rho c \frac{\partial T}{\partial t} = \nabla(K \nabla T) + Q \tag{4}$$

where ∇ represents the gradient operator in space and can be expressed as Eq. (5); ρ and K denote the density and thermal conductivity of the material, respectively; Q denotes the thermal source density; T denotes the temperature field; and t represents time.

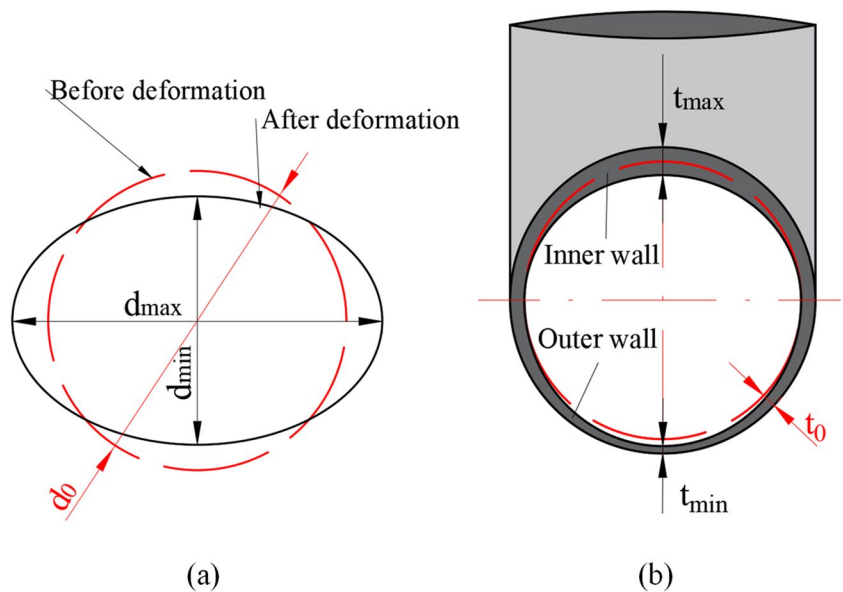
$$\nabla = \left(\frac{\partial}{\partial x}\right)i + \left(\frac{\partial}{\partial y}\right)j + \left(\frac{\partial}{\partial z}\right)k \tag{5}$$

where i , j , and k represent the unit vectors along the three coordinate axes, respectively, aligning with the positive directions of the x , y , and z axes in space.

The inside of the bent tube is cooled by cooling water, and the heat S_Q taken away by the cooling water can be expressed as Eq. (6).

$$S_Q = Km(t_2 - t_1) \tag{6}$$

Fig. 2 The schematic diagram of the ovality and wall thickness distribution of thin-walled tubes before and after deformation. **a** The ovality before and after bending. **b** The wall thickness distribution



where K represents the thermal conductivity coefficient of the die material, t_2 represents the outlet temperature, and t_1 represents the inlet temperature.

Upon achieving thermal equilibrium on the die, the tube blank is inserted, and the differential heating is achieved through direct heat transfer between the die and the tube, thereby achieving the purpose of DHP-B. In Abaqus, the heat transfer between the die and the tube is determined by the “energy rate conservation” Eq. (7) for its temperature distribution.

$$\rho c \frac{\partial \theta}{\partial t} = Q - I_q \quad (7)$$

where ρ is the density, c is the specific heat, θ is the temperature, t is the time, Q is the external heat, I_q is the internal heat.

3 Simulation of DHP-B

3.1 Mechanical properties test of 5A02 aluminum alloy at different temperatures

To obtain the material properties of 5A02 aluminum alloy, high-temperature tensile tests were conducted on the electronic universal testing machine CMT4104. The test specimens were 32 mm × 1 mm (diameter × thickness) with the sample shape and dimensions shown in Fig. 3. The tensile rates were set at 0.1 S⁻¹ and 0.01 S⁻¹, and the heating temperature ranged from 20 to 400 °C.

Figure 4 illustrates that the yield stress of the material and rheological stress decrease as the temperature increases. Additionally, the material’s rheological stress increases with an increase in strain rate.

3.2 Finite element model modeling

A finite element model for DHP-B was established based on ABAQUS, as shown in Fig. 5. Due to the prolonged heating time but relatively short duration for the bending deformation to be completed by the punch to push the tube and with a weak interaction between the temperature field and

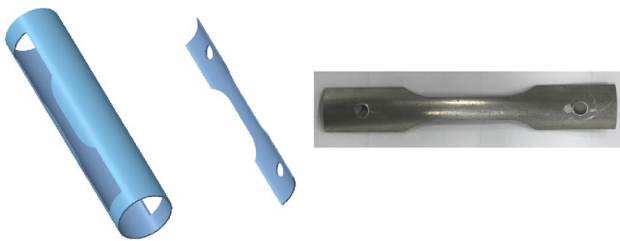


Fig. 3 Schematic diagram of high-temperature tensile test specimen

stress field, sequential thermal-mechanical coupling and the ABAQUS/standard implicit solver were therefore employed for the solution.

A 1/2 of the model is selected for simulation calculation for the symmetrical characteristic of the model. The model consists of a die, tube, punch, and elastic rubber block components. The outer side of the die bend is equipped with heating holes, while the inner side is equipped with cooling tanks. The die and punch are made of H13 steel. The grid element type of the die was defined as four-node thermal-coupled tetrahedral element C3D4T, while that of the tube was four-node thermal-coupled curved surface shell element S4RT. And a quadrilateral mesh is adopted. The punch and elastic rubber use an eight-node linear hexahedral element C3D8T.

3.3 Material model

The thermal parameters of the die and tube materials are presented in Table 1.

The cool tank is fed with water to achieve differential heating forming. Therefore, it is necessary to define the physical properties of the water. The relevant parameters are listed in Table 2.

This text employs silicone rubber as the filling material for DHP-B. Compared to ordinary polyurethane rubber, silicone rubber demonstrates exceptional elasticity and superior heat resistance [29]. The material parameters of the silicone rubber are displayed in Table 3, and its constitutive relationship adheres to the Mooney-Rivlin equation [30], encompassing material parameters C_{10} , C_{01} , and D . Among them, C_{10} and C_{01} are obtained from Eq. (8), and D is calculated from Eq. (9).

$$W = C_{10}(I_1 - 3) + C_{01}(I_2 - 3) \quad (8)$$

$$D = \frac{1 - 2\nu}{C_{10} + C_{01}} \quad (9)$$

where W is the strain energy, I_1 and I_2 are Green strain invariants, and ν is the Poisson ratio. The material parameter D characterizes the compressibility of the rubber, where D equals zero in the case of complete incompressibility. The shear behavior is described by the Rivlin coefficients C_{10} and C_{01} .

4 Simulation and analysis of factors affecting on forming

Figure 6 shows the temperature distribution during the DHP-B forming process. By examining the wall thickness distribution chart, as depicted in Fig. 7, and analyzing the

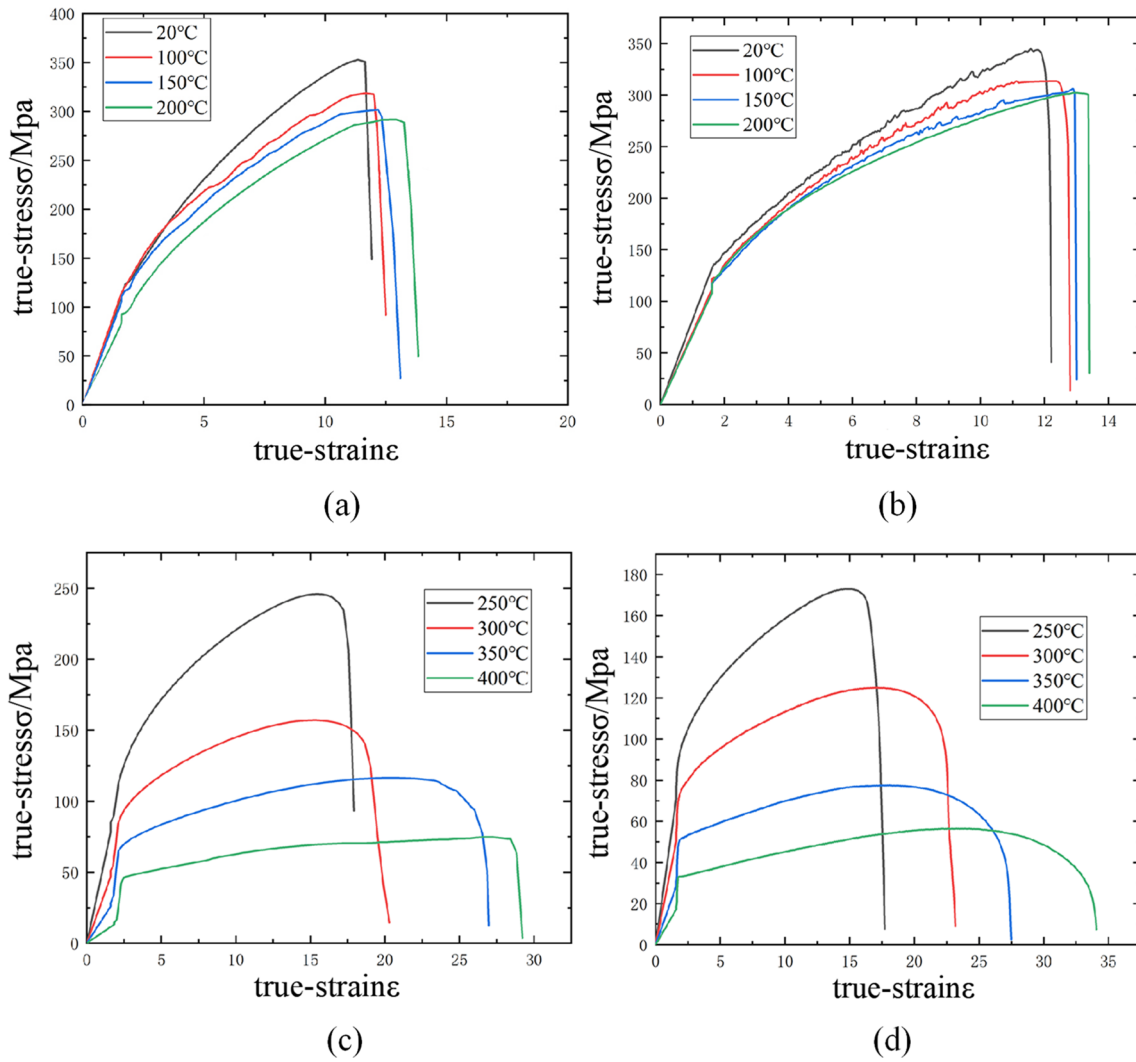


Fig. 4 True stress-strain curves at different strain rates for different heating temperatures. **a** Strain rate of 0.1 S^{-1} for heating temperatures from 20 to 200 °C . **b** Strain rate of 0.01 S^{-1} for heating temperatures

from 20 to 200 °C. **c** Strain rate of 0.1 S^{-1} for heating temperatures from 250 to 400 °C . **d** Strain rate of 0.01 S^{-1} for heating temperatures from 250 to 400 °C

Fig. 5 FEM model of DHP-B

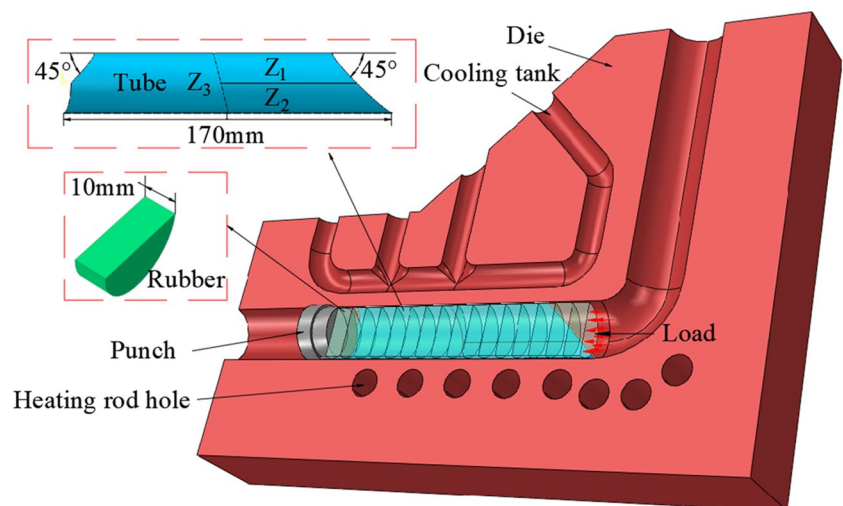


Table 1 Thermal parameters of the material

Materials	Thermal conductivity (W/mK)	Specific heat (kJ/kg °C)	Density (g/cm ³)
5A02 aluminum alloy	150.7	0.879	2.67
H13 die steel	24	0.442	7.85

Table 2 Thermophysical properties of water

Temperature (°C)	Density (kg/m ³)	Thermal conductivity ($\lambda \times 10^2$ /(W/mK))	Specific heat (kJ/kg °C)
10	999.7	57.4	4.191
20	998.2	59.9	4.183
30	995.7	61.8	4.174
40	992.2	63.5	4.174
50	988.1	64.8	4.174
60	983.1	65.9	4.179
70	977.8	66.8	4.187
80	971.8	67.4	4.195
90	965.3	68.0	4.208
100	958.4	68.3	4.220

Table 3 Material parameters of silicone rubber

C_{10}	C_{01}	ν	D
0.861	-0.777	0.499	0.0238

of the tube. The influence of DHP-B process parameters on the quality of the formed product was investigated.

4.1 Effect of temperature on forming

The bending section was divided into seven points according to angles. The thickness distribution of the intrados and extrados of the formed bent tube simulation results at different temperatures were obtained, as illustrated in Fig. 8. It is revealed that the wall thickness distribution at the intrados becomes increasingly uniform as the temperature increases. Specifically, at normal temperature (NAT) and 100 °C, the wall thickness at the intrados of the bent tube significantly increases but gradually decreases after the 45° position. This phenomenon can be attributed to the low temperature and poor material fluidity, which accumulate in the bending section. However, when the temperature reaches 300 °C, the wall thickness distribution becomes more uniform. Furthermore, the extrados experiences a reduction in thickness due to the tensile stress. Notably, the wall thickness becomes thinner as the temperature decreases, mainly due to the poor plasticity of the material and slow flow rate, which cannot be replenished in time.

4.2 Effect of friction coefficient in different zones on forming

The quality of the formed tube is directly affected by the friction during the bending process, especially the thickness distribution status. Therefore, according to the deformation

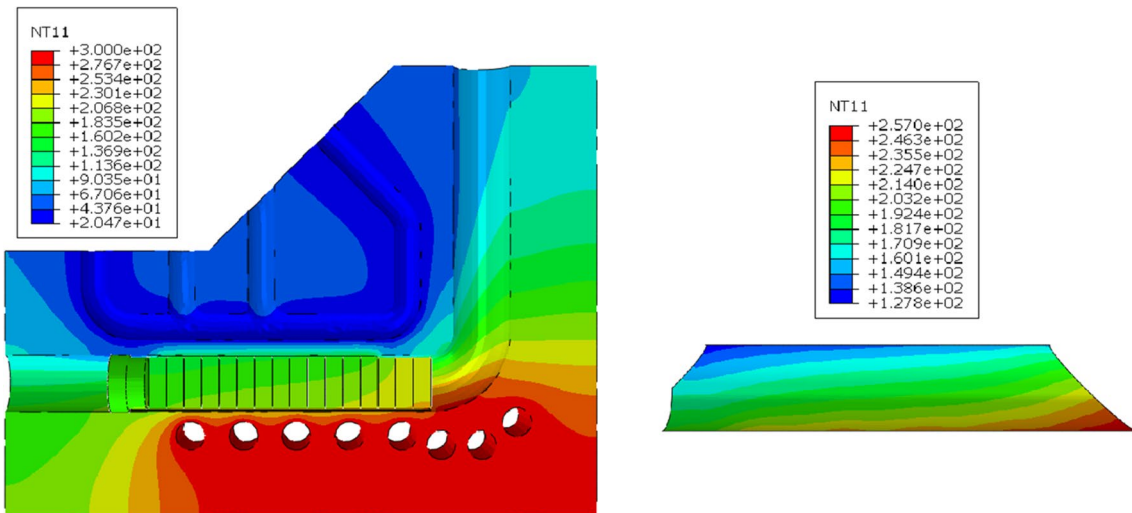
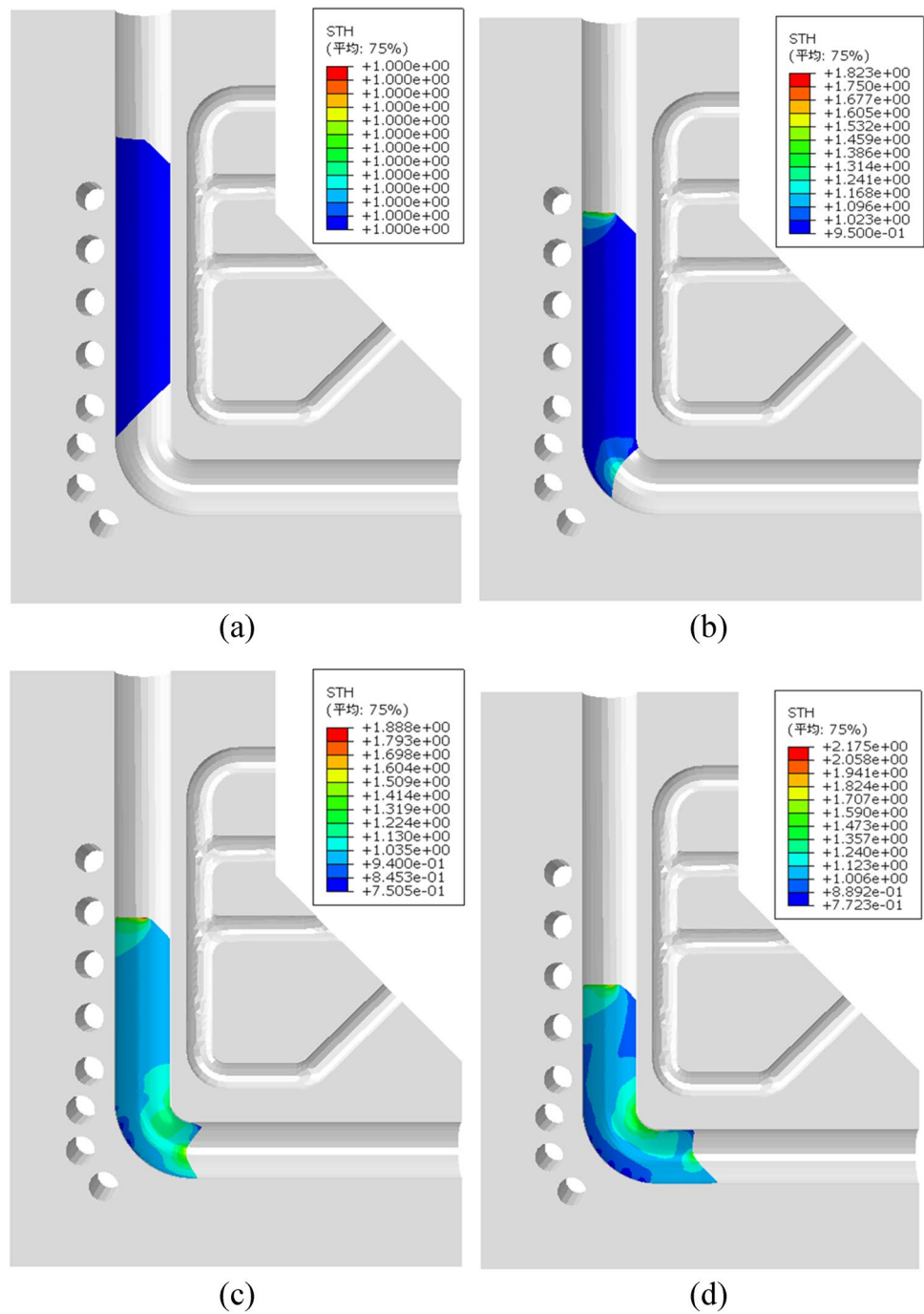


Fig. 6 Simulated temperature distribution of DHP-B

effects of temperature, friction coefficients in the inner and outer deformation zones, friction coefficients in the guide zone, reverse thrust, and other changes on the wall thickness

law of the tube during the bending process, it is divided into three parts: the inner deformation zone Z_1 , the outer

Fig. 7 Simulation of wall thickness distribution results. **a** $t=0$ s. **b** $t=4.5$ s. **c** $t=6.5$ s. **d** $t=10$ s



deformation zone Z_2 , and the guide zone Z_3 . As shown in Fig. 9, by controlling the size of the friction coefficient in each zone, the impact on the forming quality is discussed in the simulation. The lubrication scheme is shown in Table 4.

According to Fig. 10, the wall thickness first increases and then decreases at the intrados as the angle increases. Under conditions of uniform lubrication, the wall thickness gradually increases at the intrados with the increase of frictional force, but the overall thinning and uneven distribution of the wall thickness are aggravated at the extrados. The wall thickness

distribution is more uniform when differential lubrication is used. According to differential heating forming, the temperature on inner side of the bent tube is lower than that on the outer side, and the material at the intrados has better rigidity and is less prone to accumulation. So a low friction coefficient lubrication should not be used in the inner deformation zone (Z_1). Reducing the friction coefficient in the guide zone is conducive to transferring the punching force to the deformation zone of the tube and increasing the material flow rate at the intrados and extrados of the bent tube. Therefore, the tube was

Fig. 8 Curve of wall thickness with temperature in bending section

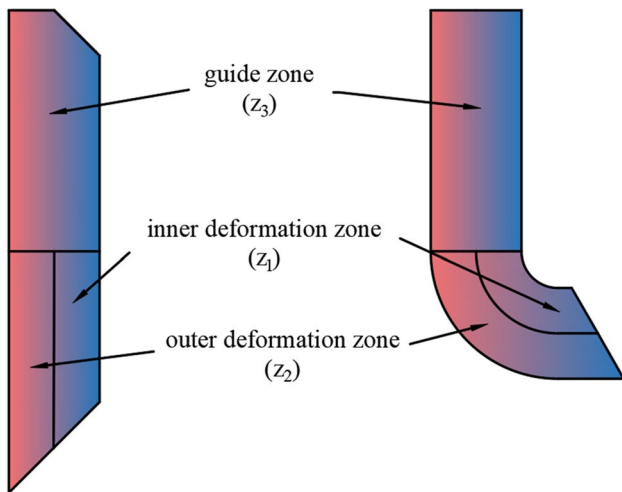
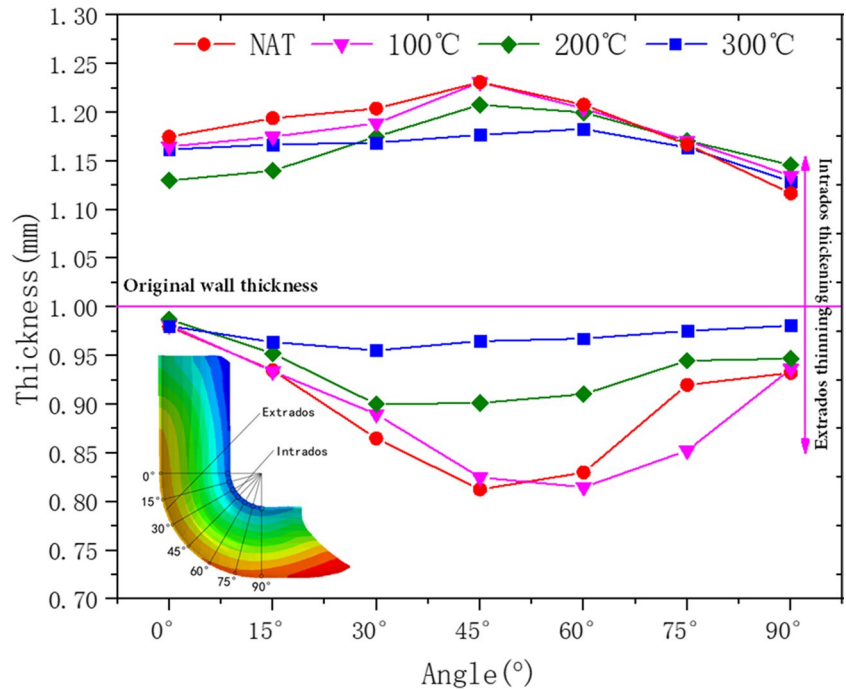


Fig. 9 Schematic diagram of tube partitioning

divided into different zones and differential lubrication was used. The material flow state in different zones of the tube can be adjusted, the distribution of wall thickness can be improved, and the forming quality can be improved.

4.3 Effect of reverse thrust on forming

Figure 11 indicates that the wall thickness increases significantly at the intrados when the reverse thrust is 27 MPa. The wall thickness distribution becomes uniform when the reverse thrust is 32 MPa; when the thrust reaches to 37 MPa and 42 MPa, the wall thickening at the intrados mainly occurs in the first half of the bending section, and the wall thickness thinning at the extrados mainly occurs in the latter half. Increasing pressure makes the material flow of the bent tube more difficult, resulting in increased wall thickening at the intrados and wall thinning at the extrados. Conversely, when the pressure is insufficient, the wall support force is insufficient, which may lead to an increased risk of ovality and wall wrinkling at the intrados. Therefore, reverse thrust is crucial for improving the wall thickness distribution and forming quality of the tube.

Table 4 Lubrication schemes for different zones

Lubrication zones		Z ₁	Z ₂	Z ₃
Uniform lubrication	Lube #1	0.1	0.1	0.1
	Lube #2	0.03	0.03	0.03
Differential lubrication	Lube #3	0.03	0.1	0.1
	Lube #4	0.1	0.1	0.03

5 Orthogonal experiment

5.1 Index of orthogonal experiment

Thinning rate, ovality, and the push-out amount are essential for bending, while the thinning rate can intuitively reflect the

Fig. 10 Curve of wall thickness with lubrication method in bending section

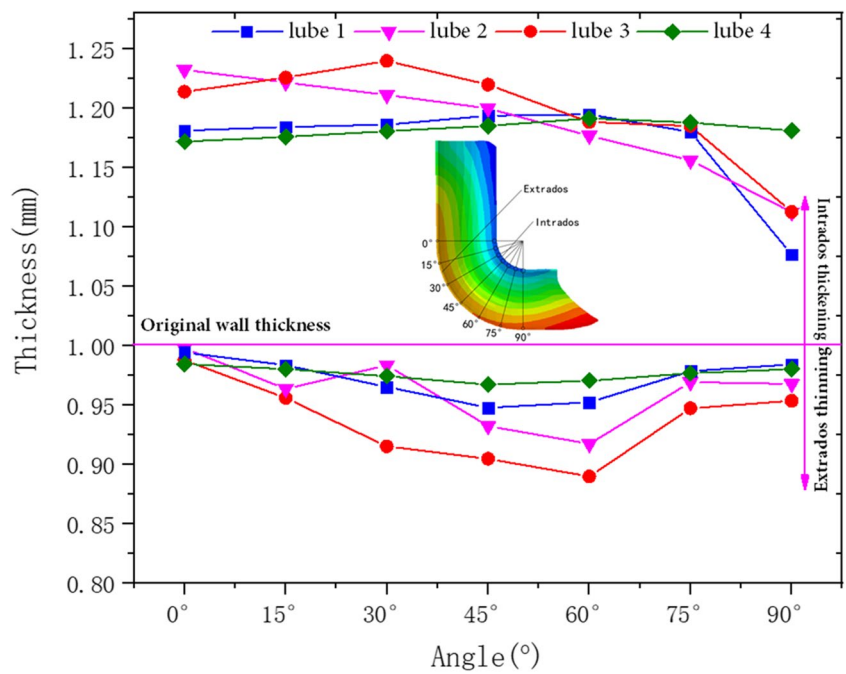
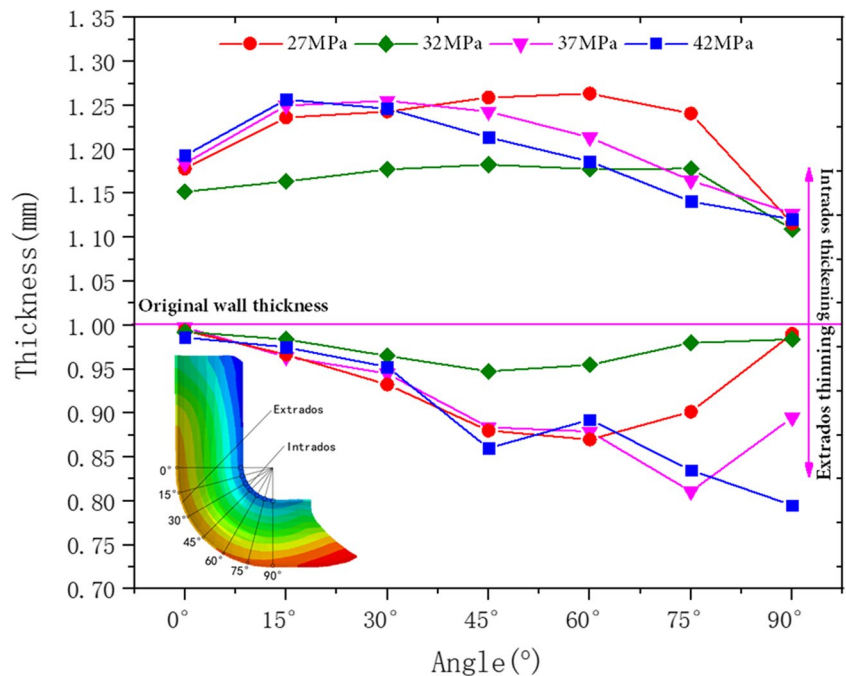


Fig. 11 Curve of wall thickness with reverse thrust in bending section



forming quality of the bent tube, ovality can describe the degree of distortion of the bent tube cross-section, and the push-out amount reflects the quality of the bending process. Without considering the interaction between various factors, range analysis can determine the primary and secondary order of the corresponding influencing factors for each index to obtain a more optimal combination of process parameters. The larger the push-out amount of the bending process, the smaller the distortion degree of the tube cross-section, and

the lower the thinning rate are desired. The factor level table in the experiments is shown in Table 5.

5.2 Range analysis results in orthogonal experiment

The experimental results have been deduced and are outlined in detail in Table 6.

Table 5 Factors and levels of orthogonal test

No.	Factor	1	2	3	4
A	Temperature/°C	100	200	300	400
B	(Z ₁) Friction coefficient	0.03	0.06	0.08	0.1
C	(Z ₂) Friction coefficient	0.03	0.06	0.08	0.1
D	(Z ₃) Friction coefficient	0.03	0.06	0.08	0.1
E	Reverse thrust/MPa	27	32	37	42

Various indicators were analyzed to obtain the optimal primary and secondary combinations for each by the comprehensive balance method. The specific experimental conclusions are presented in Tables 7, 8 and 9. The range *R* can be calculated by Eq. (10).

$$R = [\max(k_1), \max(k_2), \dots, \max(k_i)] - [\min(k_1), \min(k_2), \dots, \min(k_i)] \tag{10}$$

Table 6 Protocol and results

No.	Protocol					Results		
	A	B	C	D	E	Thinning rate/%	Ovality/%	Push-out amount/mm
1	1	1	1	1	1	8.47	2.93	21.648
2	1	2	2	2	2	7.04	4.80	15.713
3	1	3	3	3	3	8.47	4.42	10.747
4	1	4	4	4	4	5.78	1.26	0.000
5	2	1	2	3	4	8.61	5.18	12.158
6	2	2	1	4	3	11.31	6.32	12.958
7	2	3	4	1	2	2.91	4.73	14.757
8	2	4	3	2	1	5.49	6.01	14.398
9	3	1	3	4	2	7.96	4.61	12.299
10	3	2	4	3	1	5.41	3.07	12.519
11	3	3	1	2	4	9.25	5.59	11.708
12	3	4	2	1	3	3.66	4.25	12.354
13	4	1	4	2	3	4.11	4.85	10.920
14	4	2	3	1	4	3.06	4.83	12.149
15	4	3	2	4	1	7.86	6.25	13.877
16	4	4	1	3	2	9.55	3.37	13.860

Table 7 Results of range analysis for thinning rate

Metrics		A	B	C	D	E
Thinning rate	K1	29.75%	29.15%	38.59%	18.09%	27.22%
	K2	28.32%	26.82%	27.17%	25.89%	27.46%
	K3	26.29%	28.48%	24.97%	32.05%	27.55%
	K4	24.58%	24.49%	18.21%	32.91%	26.71%
	k1	7.44%	7.29%	9.65%	4.52%	6.81%
	k2	7.08%	6.70%	6.79%	6.47%	6.86%
	k3	6.57%	7.12%	6.24%	8.01%	6.89%
	k4	6.15%	6.12%	4.55%	8.23%	6.68%
<i>R</i>		1.29%	1.17%	5.10%	3.71%	0.21%
Factor priorities		C D B A E				
Optimal solution		C ₄ D ₁ B ₄ A ₄ E ₄				

where *i* is the number of factors and *k*₁, *k*₂, ..., *k*_{*i*} denote the observed values of these factors.

The varying degrees of influence on different indicators, as shown in Fig. 12, make it impractical to standardize the ranking of the importance of the impacts of five factors on three indicators. Although there are differences between the indicators, a comprehensive balancing method can be employed to derive an optimal combination of parameters.

Firstly, we analyzed the effects of the influencing factor A (temperature) on the forming, and it was concluded as follows:

- 1) For the thinning rate, the effects of A₄ and A₃ are similar.
- 2) For the ovality, A₁ is the best, followed by A₃.
- 3) For the push-out amount, A₂ has the best effect.

Table 8 Results of range analysis for ovality

Metrics		A	B	C	D	E
Ovality	<i>K1</i>	13.41%	17.57%	18.21%	16.75%	18.26%
	<i>K2</i>	22.23%	19.00%	20.47%	21.24%	17.52%
	<i>K3</i>	17.53%	21.00%	19.87%	16.04%	19.84%
	<i>K4</i>	19.30%	14.89%	13.91%	18.43%	16.85%
	<i>k1</i>	3.35%	4.39%	4.55%	4.19%	4.56%
	<i>k2</i>	5.56%	4.75%	5.12%	5.31%	4.38%
	<i>k3</i>	4.38%	5.25%	4.97%	4.01%	4.96%
	<i>k4</i>	4.82%	3.72%	3.48%	4.61%	4.21%
	<i>R</i>	2.21%	1.53%	1.64%	1.30%	0.75%
Factor priorities		C B D A E				
Optimal solution		C ₄ B ₄ D ₃ A ₁ E ₄				

Table 9 Results of range analysis for push-out amount

Metrics		A	B	C	D	E
Push-out amount	<i>K1</i>	48.108	57.025	60.174	60.908	62.442
	<i>K2</i>	54.271	53.339	54.102	52.739	56.629
	<i>K3</i>	48.880	51.089	49.593	49.284	46.979
	<i>K4</i>	50.806	40.612	38.196	39.134	36.015
	<i>k1</i>	12.027	14.256	15.043	15.227	15.610
	<i>k2</i>	13.568	13.335	13.525	13.185	14.157
	<i>k3</i>	12.220	12.772	12.398	12.321	11.745
	<i>k4</i>	12.701	10.153	9.549	9.783	9.004
	<i>R</i>	1.541	4.103	5.494	5.444	6.605
Factor priorities		E C D B A				
Optimal solution		E ₁ C ₁ D ₁ B ₁ A ₂				

However, factor A influences all three indicators. Considering the principle of reducing consumption, A₃ is chosen.

Secondly, we analyzed the effects of the influence factor B (Z₁ friction coefficient), and it was concluded as follows:

- 1) For the thinning rate and ovality, B₄ is more effective.
- 2) For the push-out amount, B₁ performs better.

However, factor B is more critical in the first two indicators and is of secondary importance regarding the push-out amount. Therefore, B₄ is the preferred choice.

Secondly, we analyzed the effects of the influence factor C (Z₂ friction coefficient), and it was concluded as follows:

- 1) For the thinning rate and ovality, C₄ performs better.
- 2) For the push-out amount, C₁ produces better results.

However, factor C is the most important of the first two indicators. Thus, C₄ is the preferred choice.

Then, we analyzed the effects of the Influence factor D (Z₃ friction coefficient) and it was concluded as follows:

- 1) For the thinning rate and push-out amount, D₁ exhibits superior performance.
- 2) For ovality, the difference between D₁ and D₃ is insignificant.

As factor D holds a significantly high degree of importance in the thinning rate, D₁ is chosen.

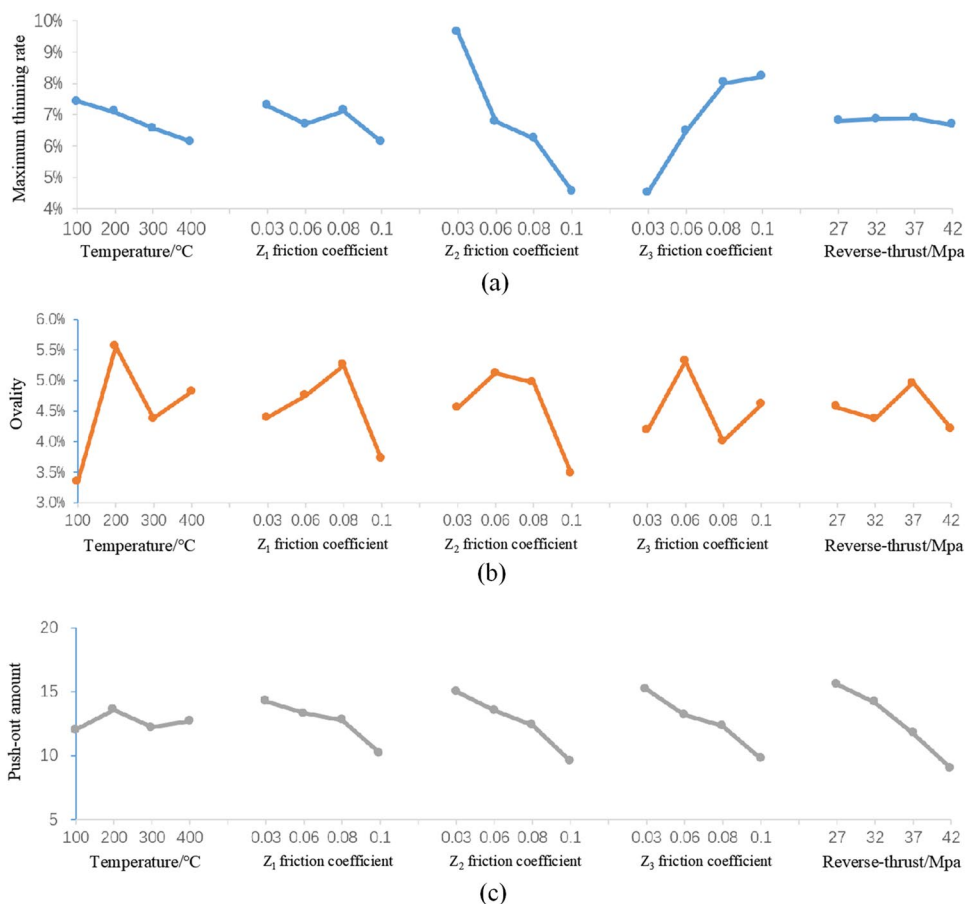
At last, we analyzed the effects of the influence factor E (reverse thrust), and it was concluded as follows:

- 1) For thinning rate and ovality, E₄ performs best.
- 2) For the push-out amount, E₁ is taken as better.

However, factor E holds the most significant position in the push-out amount. Thus, E₁ is the preferred choice.

The optimal solution has ultimately been determined as A₃B₄C₄D₁E₁, wherein the temperature is set to 300°, and the friction coefficients for the inner deformation zone (Z₁), the outer deformation zone (Z₂), and the guide zone (Z₃)

Fig. 12 Trend graphs of factors and indicators. **a** Trend graph of maximum wall thickness thinning rate indicators. **b** Trend graph of cross-sectional ovality indicators. **c** Trend graph of push-out amount indicators



are 0.1, 0.1, and 0.03, respectively, with a resulting reverse thrust of 27 MPa.

6 Experimental verification

The optimization results were validated through the finite element simulation and forming process experiments. The DHP-B experiment equipment is shown in Fig. 13. The wall thickness distribution of the model is shown in Fig. 14. After optimization, the maximum thinning rate and the cross-section ovality of the formed part were both reduced, the push-out amount increased, and the possibility of wall thickening at the intrados and wall thinning at the extrados of the bent tube was simultaneously reduced. The DHP-B experiment results are shown in Fig. 15, with Fig. 15a showing thickening and wrinkling at the intrados 1 and 2 zones and severe thinning at the extrados 1 zone. After optimizing the process parameters, the thinning rates on the intrados and extrados were reduced, and no defects, such as wrinkling or cracking, were found.

The optimized experimentally formed bent tube and simulated bent tube are equally divided into seven nodes along the bending section. The values of wall thickness for

each node are measured and compared between the simulated before and after optimization (B.O. and A.O.) and experimental values (EV), as illustrated in Fig. 16. It can be seen that the optimized simulated values are consistent with the experimental values. This indicates that the process parameters optimized through simulation and modeling have a guiding effect on improving the quality of the formed bent tube. The formed quality of the bent tube with the optimal process parameters is significantly better than other process parameters.

7 Conclusions

A differential heating push-bending (DHP-B) method for thin-walled tubes with small bending radius was proposed to improve the forming quality. The influence of temperature, friction coefficient, and reverse thrust on the forming quality was explored through orthogonal experiments. Meanwhile, DHP-B tests were carried out on 5A02 aluminum alloy tubes with a diameter of 32 mm, a wall thickness of 1 mm, and a relative bending radius of 0.9. The experimental results were consistent with the simulation results. The conclusions are as follows:

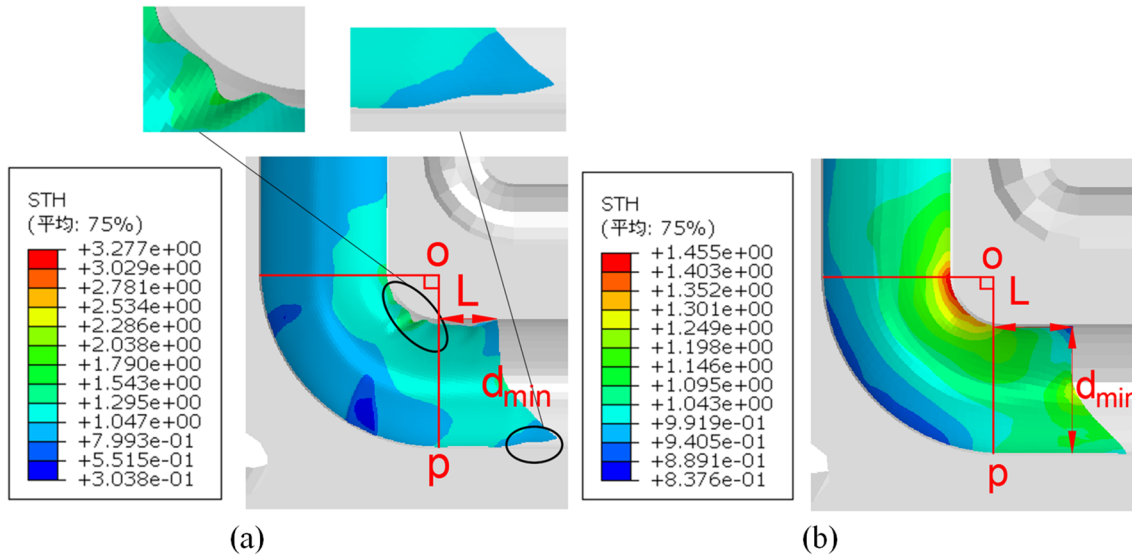


Fig. 13 Simulation results of DHP-B. **a** Before optimization of process parameters. **b** After optimization of process parameters

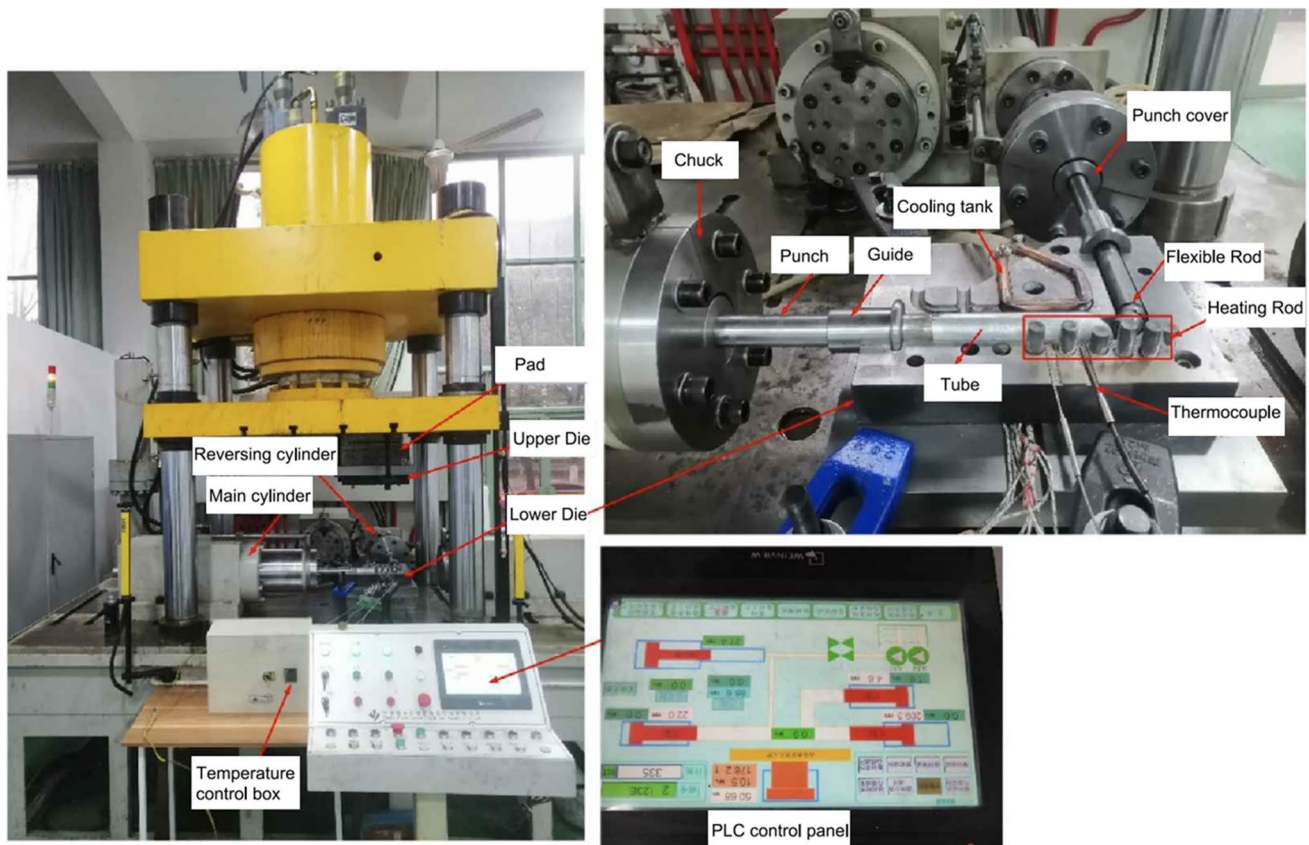


Fig. 14 Experimental unit of DHP-B

(1) Based on the influence of temperature difference on the thickness distribution of the bent tube, the optimum temperature is 300 °C. Higher temperatures accelerated the flow of materials, leading to an

increase in the thickening rate and a decrease in the thinning rate of the bent tube. Furthermore, higher temperatures caused a reduction in the strength of the rubber, resulting in inadequate support and an

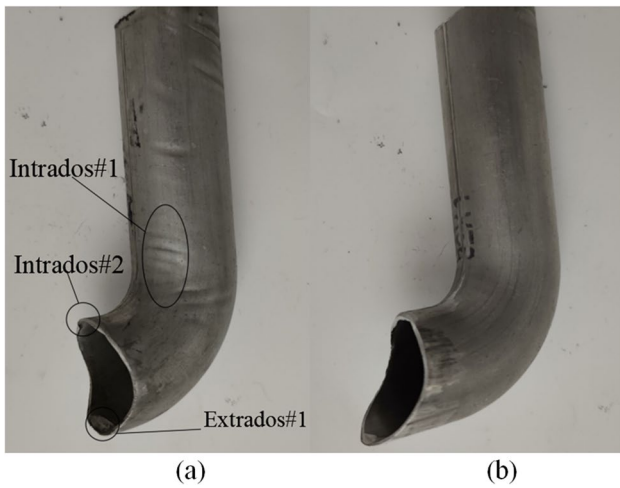


Fig. 15 The tubes bent with differential heating method. **a** Before optimization of process parameters. **b** After optimization of process parameters

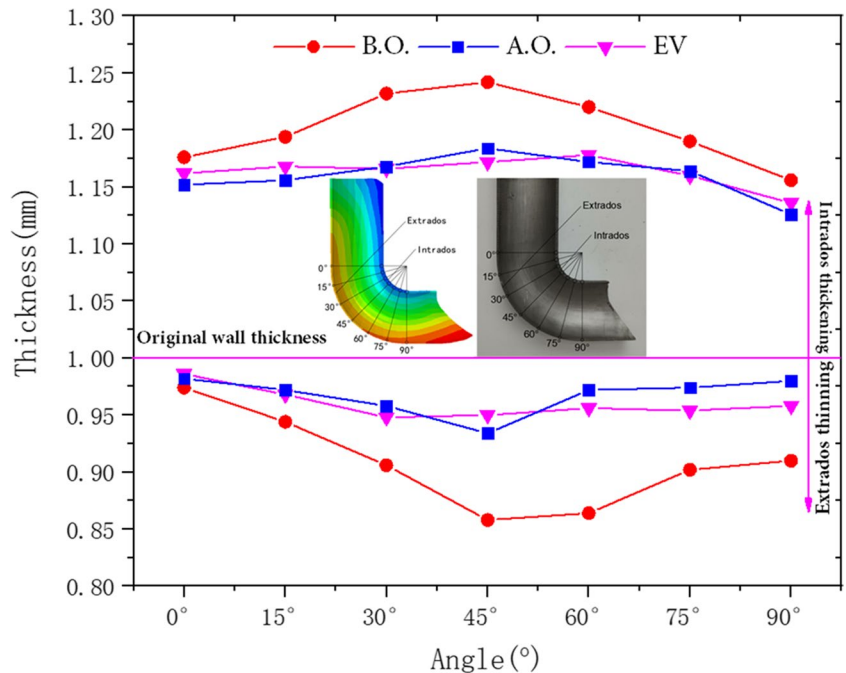
increase in the ovality of the bent tube. Lower temperatures may induce uneven wall thickness distribution in the bent tube due to decreased material plasticity, reduced fluidity, and increased accumulation at the bend section.

- (2) When performing differential heating forming, reducing the friction coefficient within the guiding zone (Z_3)

of the tube and increasing the differentiation of lubrication methods between the inner and outer deformation zones of the tube (Z_1 and Z_2) can be advantageous in facilitating the transmission of thrust towards the deformation zone. It results in the increasing flow velocity of material on the inner and outer sides of the tube, which reduces the likelihood of material accumulation and subsequently decreases the wall thickening at the intrados and wall thinning at the extrados of the bent tube.

- (3) Reverse thrust facilitates the distribution of the wall thickness in bending tubes and improves the quality of tube forming; short reverse thrust may result in inadequate internal pressure, leading to wrinkling during bending; excessive reverse thrust may cause material accumulation and increase the risk of wrinkling on the intrados and fracture on the extrados of the bent tube.
- (4) The optimal solution obtained through orthogonal experiments is $A_3B_4C_4D_1E_1$, i.e., the temperature of 300 °C, the friction coefficient of 0.1 in the Z_1 zone, 0.1 in the Z_2 zone, 0.03 in the Z_3 zone, and reverse thrust of 27 MPa. With this scheme, the forming quality of the tube is stable, without any defects such as wrinkling or over-thinning; the cross-sectional ovality is low; and the wall thickness distribution is more reasonable.

Fig. 16 Thickness distribution of the bending section of the simulation and experimental results



Acknowledgements The authors thank the financial supports from the National Natural Science Foundation of China with Grant (NO. 52265052), National Science and Technology Major Project of China (No. J2019-VII-0014-0154), and National Defense Key Disciplines Laboratory of Light Alloy Processing Science and Technology of Nanchang Hangkong University (NO. EG201903452).

Author contribution Mingliang Peng: writing, experiment. Xuefeng Xu: conceptualization, methodology. Yubin Fan: writing—review, validation. Jie Xiao: revision, validation. Liming Wei: data processing. Jun Xie: software. Dong Yang: experiment.

Funding This work was supported by the National Natural Science Foundation of China with Grant (NO. 52265052), National Natural Science Foundation of China with Grant (NO. 51975267), National Science and Technology Major Project of China (No. J2019-VII-0014-0154), and Natural Science Foundation of Jiangxi, China (No. 20224BAB214050).

Data availability All the data have been presented in the manuscript.

Code availability Not applicable.

Declarations

Ethics approval Not applicable.

Consent to participate Not applicable.

Consent for publication Not applicable.

Competing interests The authors declare no competing interests.

References

- Yang H, Li H, Zhang Z, Zhan M, Liu J, Li G (2012) Advances and trends on tube bending forming technologies. *Chin J Aeronaut* 25(1):1–12. [https://doi.org/10.1016/s1000-9361\(11\)60356-7](https://doi.org/10.1016/s1000-9361(11)60356-7)
- Liu H, Zhang SH, Song HW, Shi GL, Cheng M (2019) 3D FEM-DEM coupling analysis for granular-media-based thin-wall elbow tube push-bending process. *Int J Mater Form* 12(6):985–994. <https://doi.org/10.1007/s12289-019-01473-8>
- Oh IY, Han SW, Woo YY, Ra JH, Moon YH (2018) Tubular blank design to fabricate an elbow tube by a push-bending process. *J Mater Process Technol* 260:112–122. <https://doi.org/10.1016/j.jmatprotec.2018.05.017>
- Zhou WB, Shao ZT, Yu JQ, Lin JG (2021) Advances and trends in forming curved extrusion profiles. *Materials* 14(7):29. <https://doi.org/10.3390/ma14071603>
- Limam A, Lee LH, Corona E, Kyriakides S (2010) Inelastic wrinkling and collapse of tubes under combined bending and internal pressure. *Int J Mech Sci* 52(5):637–647. <https://doi.org/10.1016/j.ijmecsci.2009.06.008>
- Zhang X, Zhao CC, Du B, Chen D, Li Y, Han ZJ (2021) Research on hydraulic push-pull bending process of ultra-thin-walled tubes. *Metals* 11(12):14. <https://doi.org/10.3390/met11121932>
- Xu J, Yang H, Li H, Zhan M (2012) Significance-based optimization of processing parameters for thin-walled aluminum alloy tube NC bending with small bending radius. *Trans Nonferrous Met Soc China* 22(1):147–156. [https://doi.org/10.1016/s1003-6326\(11\)61154-0](https://doi.org/10.1016/s1003-6326(11)61154-0)
- Zhang Z, Yang JC, Huang WL, Ma J, Li H (2021) Uncertainty analysis and robust design optimization for the heat-assisted bending of high-strength titanium tube. *Sci China-Tech-nological Sci* 64(10):2174–2185. <https://doi.org/10.1007/s11431-021-1881-8>
- Xu Y, Lv XW, Wang Y, Zhang SH, Xie WL, Xia LL, Chen SF (2023) Effect of hot metal gas forming process on formability and microstructure of 6063 aluminum alloy double wave tube. *Materials* 16(3):15. <https://doi.org/10.3390/ma16031152>
- Zhang ZY, Yang H, Li H, Ren N, Tian YL (2011) eBending behaviors of large diameter thin-walled CP-Ti tube in rotary draw bending. *Progress Nat Science-Materials Int* 21(5):401–412. [https://doi.org/10.1016/s1002-0071\(12\)60076-8](https://doi.org/10.1016/s1002-0071(12)60076-8)
- Zhang XL, Yang H, Li H, Zhang ZY, Li L (2014) Warm bending mechanism of extrados and intrados of large diameter thin-walled CP-Ti tubes. *Trans Nonferrous Met Soc China* 24(10):3257–3264. [https://doi.org/10.1016/s1003-6326\(14\)63465-8](https://doi.org/10.1016/s1003-6326(14)63465-8)
- Wu WY, Zhang P, Zeng XQ, Jin L, Yao SS, Luo AA (2008) Bendability of the wrought magnesium alloy AM30 tubes using a rotary draw bender. *Mater Sci Eng a-Structural Mater Prop Microstruct Process* 486(1–2):596–601. <https://doi.org/10.1016/j.msea.2007.09.033>
- Wu WY, Jin L, Dong J, Peng LM, Yao SS (2010) Bending mechanisms in AM30 alloy tube using a rotary draw bender. *Mater Manuf Processes* 25(12):1359–1364. <https://doi.org/10.1080/10426911003636928>
- Tao Z, Li H, Ma J, Yang H, Lei C, Li G (2017) FE modeling of a complete warm-bending process for optimal design of heating stages for the forming of large-diameter thin-walled Ti–6Al–4V tubes. *Manufacturing Review* 4.
- Li XT, Wang MT, Du FS, Xu ZQ (2006) FEM simulation of large diameter pipe bending using local heating. *J Iron Steel Res Int* 13(5):25–29. [https://doi.org/10.1016/s1006-706x\(06\)60090-3](https://doi.org/10.1016/s1006-706x(06)60090-3)
- Chavoshi SE, Torshizi SEM (2019) Bending improvement in spot heating of pipes in comparison with line heating method. *Mech Ind* 20(4):9. <https://doi.org/10.1051/meca/2019030>
- Trần R, Reuther F, Winter S, Psyk V (2020) Process development for a superplastic hot tube gas forming process of titanium (Ti–3Al–2.5V) hollow profiles. *Metals* 10(9):12. <https://doi.org/10.3390/met10091150>
- Hoffmann E, Meya R, Tekkaya AE (2021) Reduction of warping in kinematic L-profile bending using local heating. *Metals* 11(7):19. <https://doi.org/10.3390/met11071146>
- Yan J (2016) Plastic wrinkling model and characteristics of shear enforced Ti-alloy thin-walled tubes under combination die constraints and differential temperature fields. *Chin J Aeronaut* 29(6):1815–1829. <https://doi.org/10.1016/j.cja.2016.06.019>
- Yan J, Wu W, Xu BT (2017) Prediction for multi-index constrained forming limit in shear bending process of Ti-alloy thin-walled tube under differential temperature fields. *Int J Adv Manuf Technol* 91(1–4):1117–1128. <https://doi.org/10.1007/s00170-016-9791-x>
- Hu Z (2000) Elasto-plastic solutions for spring-back angle of pipe bending using local induction heating. *J Mater Process Tech* 102
- Vorkov V, Arola AM, Larkkiola J, Vandepitte D, Dufloou JR (2018) Influence of radiant heating on air bending. *Int J Adv Manuf Technol* 97(1–4):1421–1429. <https://doi.org/10.1007/s00170-018-2036-4>
- Schlemmer KL, Osman FH (2005) Differential heating forming of solid and bi-metallic hollow parts. *J Mater Process Technol* 162:564–569. <https://doi.org/10.1016/j.jmatprotec.2005.02.124>
- Liu G, Zhang WD, He ZB, Yuan SJ, Lin Z (2012) Warm hydro-forming of magnesium alloy tube with large expansion ratio within non-uniform temperature field. *Trans Nonferrous Met Soc China* 22:S408–S415. [https://doi.org/10.1016/s1003-6326\(12\)61739-7](https://doi.org/10.1016/s1003-6326(12)61739-7)
- Guo XZ, Jin K, Wang H, Pei WJ, Ma FY, Tao J, Kim N (2016) Numerical simulations and experiments on fabricating bend pipes

- by push bending with local induction-heating process. *Int J Adv Manuf Technol* 84(9–12):2689–2695. <https://doi.org/10.1007/s00170-015-7898-0>
26. Simonetto E, Venturato G, Ghiotti A, Bruschi S (2018) Modelling of hot rotary draw bending for thin-walled titanium alloy tubes. *Int J Mech Sci* 148:698–706. <https://doi.org/10.1016/j.ijmecsci.2018.09.037>
27. Yang H, Li H, Ma J, Li G, Huang D (2021) Breaking bending limit of difficult-to-form titanium tubes by differential heating-based reconstruction of neutral layer shifting. *Int J Mach Tools Manuf* 166:20. <https://doi.org/10.1016/j.ijmachtools.2021.103742>
28. Cheng JW, Song G, Zhang ZD, Khan MS, Liu ZF, Liu LM (2022) Improving heat-affected zone softening of aluminum alloys by in-situ cooling and post-weld rolling. *J Mater Process Technol* 306:15. <https://doi.org/10.1016/j.jmatprotec.2022.117639>
29. Shit SC, Shah P (2013) A review on Silicone Rubber. *Natl Acad Sci Letters-India* 36(4):355–365. <https://doi.org/10.1007/s40009-013-0150-2>
30. Keerthiwansa R, Javorik J, Kledrowetz J, Nekoksa P (2018) Elastomer testing: the risk of using only uniaxial data for fitting the mooney-rivlin hyperelastic-material model. *Materiali Tehnologije* 52(1):3–8. <https://doi.org/10.17222/mit.2017.085>

Publisher's Note Springer Nature remains neutral with regard to jurisdictional claims in published maps and institutional affiliations.

Springer Nature or its licensor (e.g. a society or other partner) holds exclusive rights to this article under a publishing agreement with the author(s) or other rightsholder(s); author self-archiving of the accepted manuscript version of this article is solely governed by the terms of such publishing agreement and applicable law.